

# Laser bandwidth effect on overlay budget and imaging for the 45 nm and 32nm technology nodes with immersion lithography

Umberto Iessi<sup>a</sup>, Michiel Kupers<sup>b</sup>, Elio De Chiara<sup>a</sup>, Pierluigi Rigolli<sup>a</sup>, Ivan Lalovic<sup>c</sup>, G. Capetti<sup>a</sup>

<sup>a</sup>Numonyx, Via C. Olivetti 2, Agrate Brianza (MI) 20041, Italy

<sup>b</sup>Cymer B.V., De Run 4312B, 5503 LN Veldhoven, Netherlands

<sup>c</sup>Cymer, Inc., 17075 Thornmint Court, San Diego, CA 92127

## ABSTRACT

The laser bandwidth and the wavelength stability are among the important factors contributing to the CD Uniformity budget for a 45 nm and 32nm technology node NV Memory. Longitudinal chromatic aberrations are also minimized by lens designers to reduce the contrast loss among different patterns. In this work, the residual effect of laser bandwidth and wavelength stability are investigated and quantified for a critical DOF layer. Besides the typical CD implications we evaluate the “image placement error” (IPE) affecting specific asymmetric patterns in the device layout. We show that the IPE of asymmetric device patterns can be sensitive to laser bandwidth, potentially resulting in nanometer-level errors in overlay. These effects are compared to the relative impact of other parameters that define the contrast of the lithography image for the 45nm node. We extend the discussion of the contributions to IPE and their relative importance in the 32 nm double-patterning overlay budget.

Keywords: CD Uniformity, Overlay Budget, Lens Aberrations, Laser bandwidth, Image Placement error

## 1. INTRODUCTION

As the industry heads towards ever smaller feature sizes and complex pattern layouts, sources of imaging and overlay errors that were neglected in the past are now becoming increasingly significant. In this paper we will investigate the impact of laser bandwidth on CD and the image placement error of asymmetric device patterns. Although the CD imaging effects have been explored before, for example in a paper by Bisschop et. al. (see reference [3]), here we will apply methods to specifically quantify the image placement effects for specific asymmetric device patterns for NV Memory (see reference [1]). This pattern was printed with a 6%-attenuated Phase Shift Mask at NA=1.20 using dipole illumination at 193nm wavelength. The dipole was horizontally oriented and had 60-deg opening angle, radially delimited by SigmaInner=0.65, SigmaOuter=0.85. The exposure-light was polarized in y-direction.

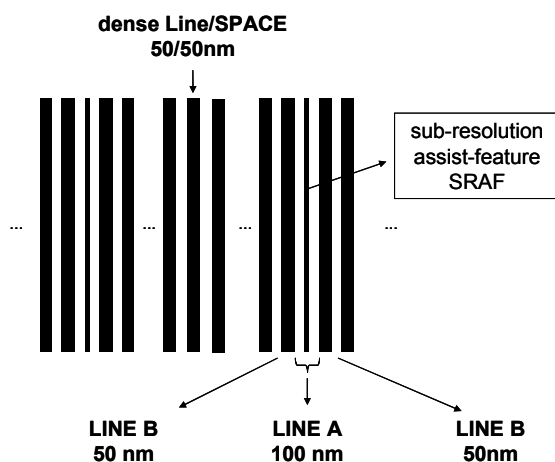
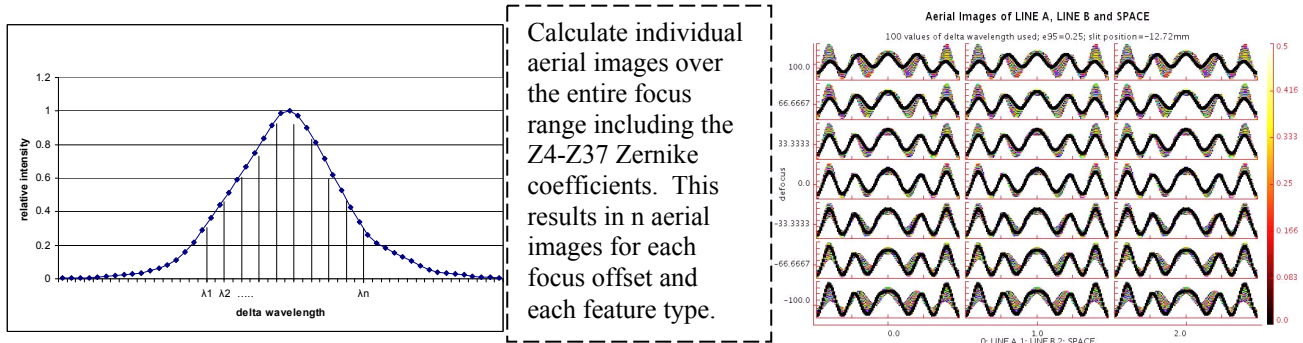


Figure 1: Pattern to be printed: Dense lines and spaces with pitch-interruption. Investigated are Critical Dimensions CD of ‘LINE A’, ‘LINE B’ and ‘SPACE’. Dimensions indicated in the figure are target-values.

Furthermore, we will use simulation software to study the impact of laser bandwidth on CD as well as on the Image Placement Error (IPE) and the relative contributions of the higher order Zernike coefficients. A recent update in the Panoramic™ lithography simulation software now makes it possible to directly calculate the impact of the higher-order chromatic aberrations. The resulting aerial image is calculated by sampling the spectrum at discrete wavelength points. A set of aerial images is obtained with each image corresponding to a single wavelength sample. Finally, the images are weighted by the intensity in the laser spectrum at the corresponding wavelength and summed together. This computation method has been described before, for example references [3,4], and is described schematically in the figure below. In our case, the individual aerial images are computed with different aberration levels as defined by a set of Z4-Z37 Zernike coefficients corresponding to each discrete wavelength sample.



In this study, the aggregate aerial image is calculated using a typical spectrum from a Cymer XLA360 laser, which is shown in Figure 2.

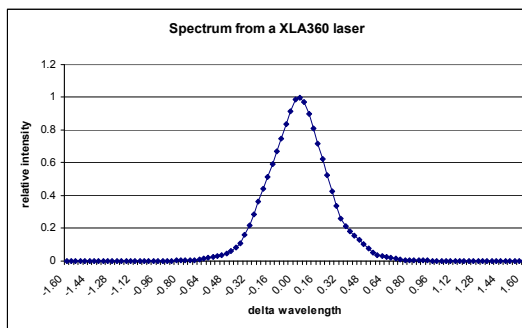


Figure 2 XLA360 spectrum used as a weighting function for the simulations.

A previous study has quantified the effect of IPE as a function different overlay marks (see reference [2]). Although these effects are quite small, we have extended this work to study the effect of the higher order chromatic aberrations for the AIM overlay marks used for this particular layer

## 1.1 Impact of higher order aberrations on IPE

Higher order aberrations are commonly defined as the Z5 to Z37 Zernike polynomial terms that describe deformations from spherical wavefronts (see for example reference [6]). In prior studies, it has been shown that the IPE is mostly affected by the lower order terms and it was assumed that higher order terms are small and can be neglected. Our simulation will quantify the magnitude of the contributions of the higher order terms for the particular features described above.

## 2. SIMULATIONS

### 2.1 IPE simulations for 45 nm node

For our simulations we will use Hyperlith™ from Panoramic Inc. The following inputs were used:

- GDS data from the reticle using 0.5 nm of simulation grid
- NA: 1.2 ; sigma inner=0.85 sigma outer=0.65, using X 60° dipole (Y polarized)
- Used -350 nm/pm as chromatic sensitivity

- Used measured Zernike data at 3 wavelengths (0, -0.5pm, +0.5pm) from an ASML XT1700i scanner in the Numonyx Fab. Due to confidentiality reasons we will not disclose the exact numbers.
- +/- 10% and +/- 100 nm of aerial image threshold and focus variation applied respectively.
- The image threshold is anchored to the SPACE feature

The results are shown in the plots of Figure 3 and Figure 4. Note that the plots are a function of focus and slit position. Except for LINE A, the variation of the IPE in the slit due to the higher order Zernikes is quite small. LINE B is more sensitive to focus variations than LINE A. In Figure 4 we show the variation of the IPE through the slit for the different types of pattern. These values are confirmed by an overlay experiment, and we discuss these results in section 3.4.

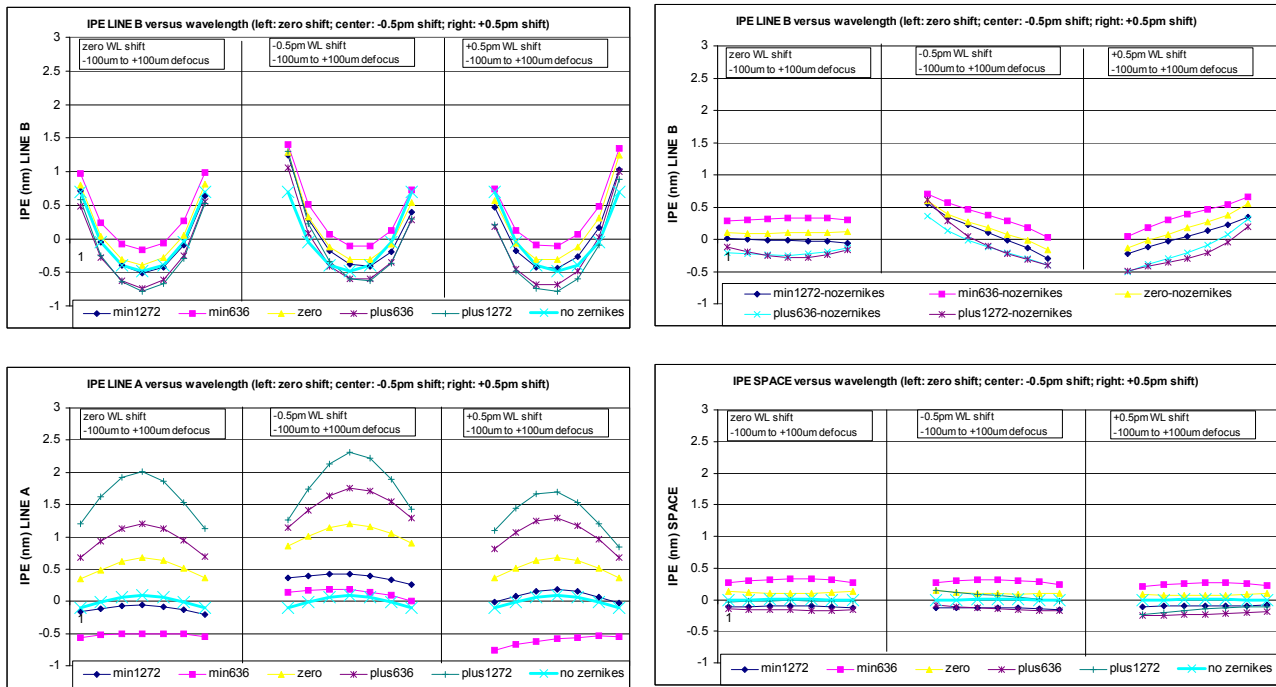


Figure 3: IPE (nm) through focus, slit position, wavelength and feature type. The wavelength of the laser was changed by -0.5pm and +0.5pm. From left to right and top to bottom: IPE LINE B through focus and wavelength; the change in IPE through focus when the no Zernike case is subtracted; IPE LINE A through focus and wavelength; IPE SPACE through focus and wavelength

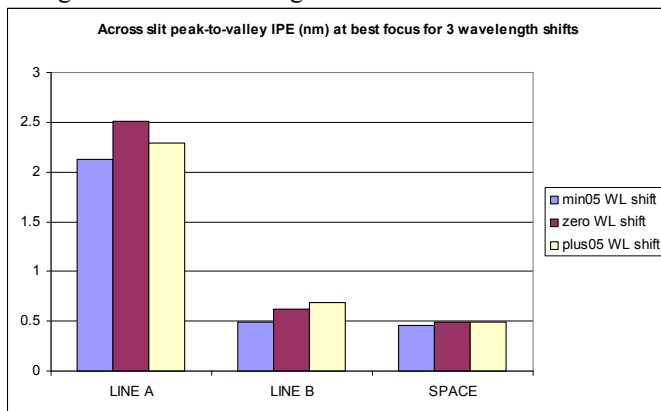


Figure 4 : total IPE variation over the slit for 3 types of patterns

To investigate the effect of chromatic aberrations and finite laser bandwidth on IPE, we will now generalize this approach and consider the aggregate aerial images computed over a range of wavelengths. To do this we must obtain the Zernike coefficients as a function of wavelength. The Zernike sensitivities to wavelength for this optical lithography scanner were determined experimentally, by measuring the aberrations at several wavelength set-points. These Zernike coefficients are typically linear with the wavelength, over a range of several picometers of wavelength offsets from nominal, which means we can perform interpolation to determine a range of intermediate values. Previous studies (reference [3] and [7]) have discussed the sampling requirements in order to accurately simulate the effect of bandwidth when using the defocus or Z4 aberration term only. Since it is rather easy to program the number of interpolations in the simulation software we have chosen to interpolate and calculate the aggregate aerial image over 100 samples of wavelength shift. We also consider 6 values of the E95 laser bandwidth: 0.00pm, 0.25pm, 0.32pm, 0.38pm, 0.50pm and 1.00pm. We have included the  $e_{95}=1.0\text{pm}$  value in order to assess the effect of bandwidth significantly beyond the usual operating range of lasers such as the XLA360 (see section 3.4 for a discussion on this).

To get an accurate description of the behavior of IPE versus bandwidth with and without the higher order Zernikes, we will compute the IPE at 5 different positions in the slit as well as through focus (-100um to +100um). The results for LINE B are plotted in Figure 5. Similar plots can be made for the other features. Figure 6 and Figure 7 show the IPE at best focus for LINE B, LINE A and SPACE for all the E95 values as well as the case where the Zernike coefficients are absent from the simulation. We see that LINE B is most sensitive to bandwidth whereas LINE A is mostly sensitive to the higher order Zernikes. In Figure 8 we show the variation of IPE over the slit as a function of bandwidth when we also consider the impact of the lower order Zernikes (Z2, Z3, Z4). From Figure 5 we see that the IPE for the most sensitive pattern, LINE B, changes by 0.9nm to 1.5 nm (depending on focus) over the 1pm change in BW. The other patterns are not sensitive to bandwidth. Note that the IPE effect is significantly lower over the typical bandwidth operating ranges of the XLA 360 laser, namely about 0.2nm to 0.5nm at extremes of defocus. The effect is even lower for laser systems that feature active bandwidth stabilization, such as the XLR 560i.

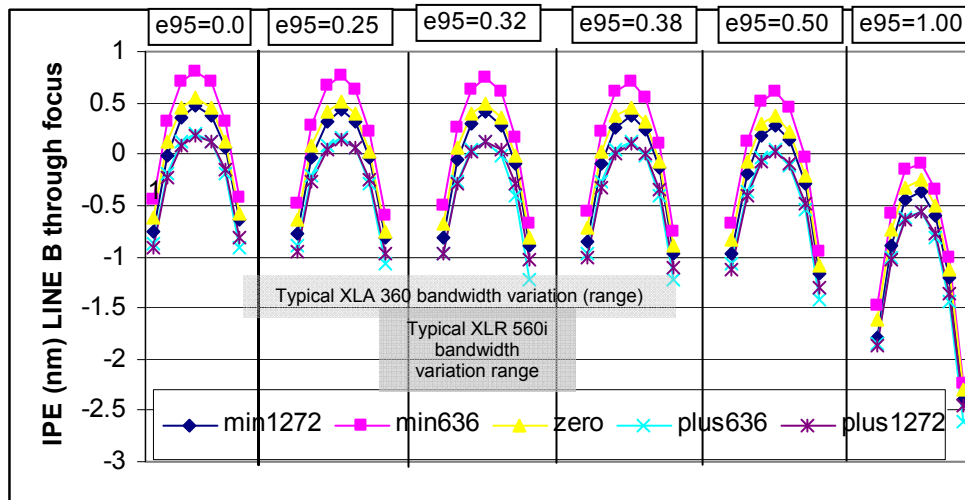


Figure 5: IPE as a function of laser bandwidth for LINE B through focus (-100nm, -66nm, -33nm, 0, +33nm, +66nm, +100nm)

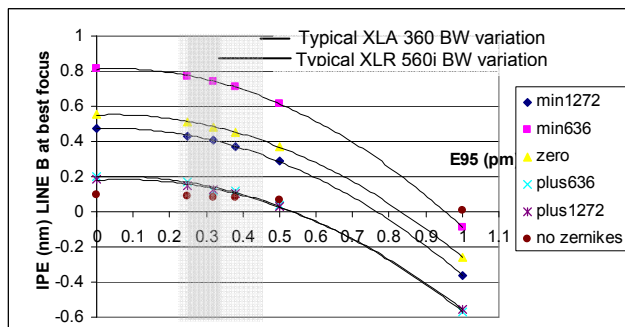


Figure 6: IPE as a function of bandwidth for LINE B. The bandwidth variation range for the XLA 360 laser type used in these experiments is shown in the shaded area; the typical bandwidth variation for XLR 560i systems featuring advanced bandwidth stabilization is also included for comparison

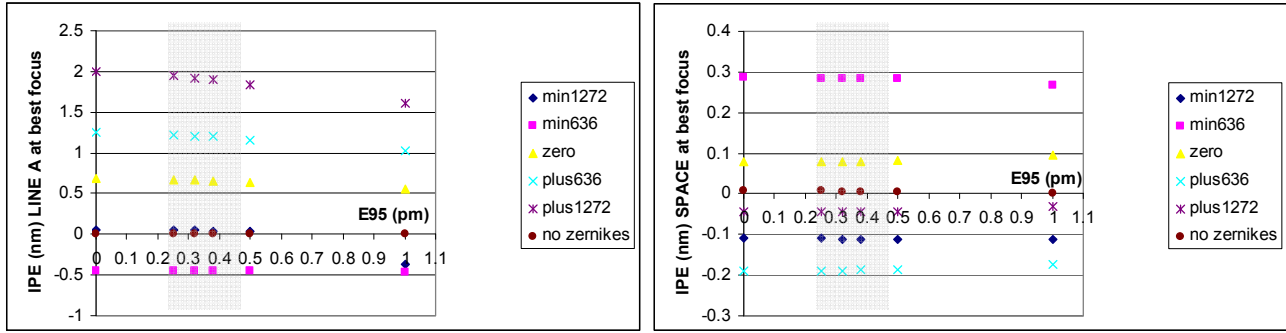


Figure 7: IPE as a function of laser bandwidth for LINE A and SPACE. The bandwidth variation range for the XLA 360 laser type used in these experiments is shown in the shaded area

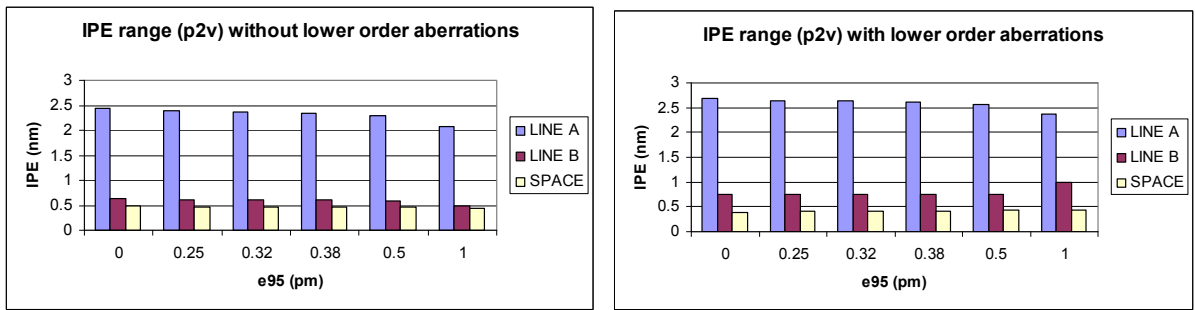


Figure 8: Across-slit IPE range at best focus with and without the lower order aberrations as a function of laser bandwidth for LINE A, LINE B and SPACE

## 2.2 IPE simulations for 32 nm node

The 32 nm lithography step for NV Memories require the introduction of Self Align Double Patterning (SADP) methods. With this technique, it could be necessary to print asymmetric patterns in order to obtain the final desired structure after spacer definition. In our case study we evaluate the IPE of a pattern named “L” (see Figure 9) with different lens NA :1.2 immersion and 0.93 dry.

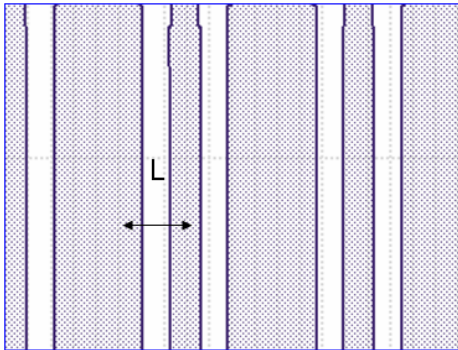


Figure 9: asymmetric layout for a 32nm technology node SADP memory device

The lithography pitch for a 64 nm SADP device is the half of the final patterned one so that dry lithography can be sufficient. Figure 10 shows that IPE is less than 0.2 nm and it is not sensitive to defocus. The relaxed k1 factor for both dry and immersion process (0.31 and 0.4 respectively) is protecting this technology node from IPE issues.

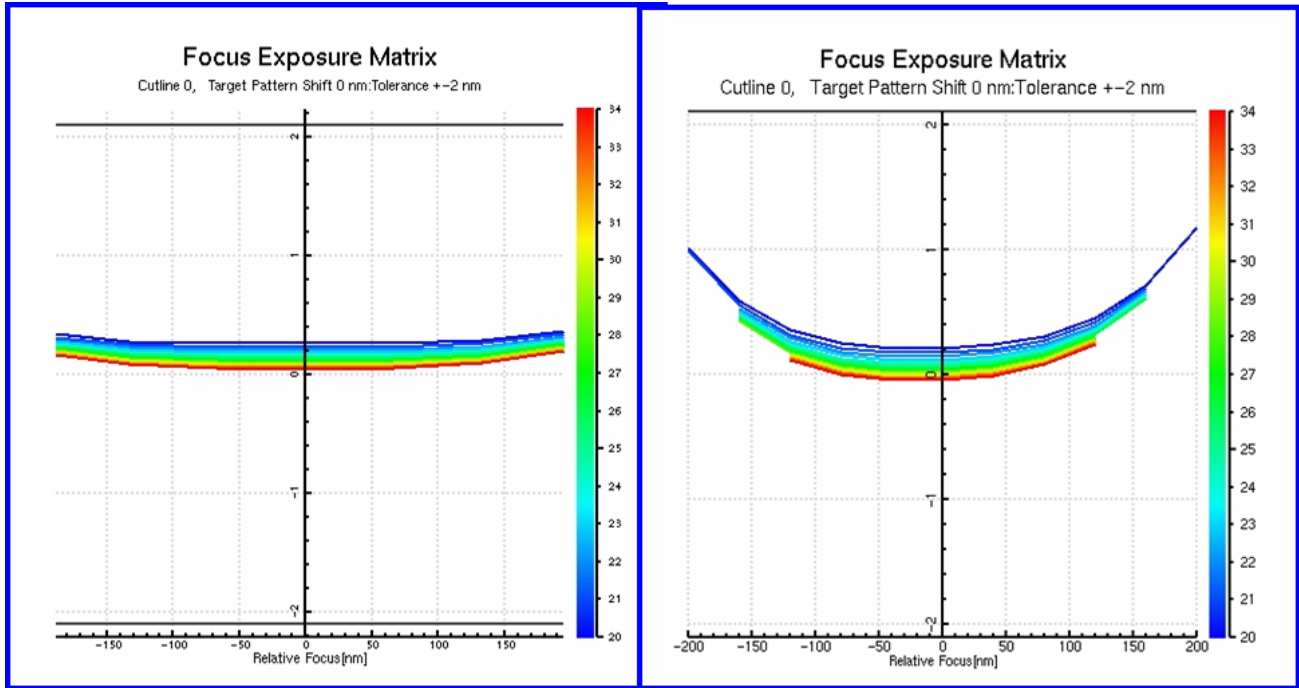


Figure 10: IPE(nm) through focus for the "L" pattern at different exposure doses

### 2.3 CD Uniformity simulations for 45 nm node

In order to evaluate the impact of laser bandwidth on our critical patterns we use ASML LithoCruiser Software to run simulations including in the model the appropriate scanner lens and illuminator fingerprint and a calibrated resist model.

This software first calculates the sensitivities of critical patterns to the main scanner parameters and then estimates a CDU budget for each of these main contributors in an early immersion lithography litho cell.

	Line A 3 $\sigma$ (nm)	Line B 3 $\sigma$ (nm)	Space 3 $\sigma$ (nm)
<b>All</b>	<b>3.05</b>	<b>2.78</b>	<b>2.30</b>
<b>Scanner</b>	0.52	0.83	0.26
<b>Laser</b>	<b>0.91</b>	<b>0.07</b>	<b>0.44</b>
<b>Reticle</b>	2.27	2.00	1.41
<b>Process</b>	1.51	1.51	1.51
<b>Other</b>	0.88	0.87	0.87

Table 1: CD uniformity for LINE A, LINE B and SPACE for each main contributor

The laser bandwidth contribution sensitivity is calculated by varying the bandwidth FWHM around the nominal value of 0.12 pm (equivalent to  $e95=0.25\text{pm}$ ) and considering the defocus term only.

The laser bandwidth FWHM is varied over a range of 0.04 pm (0.08pm to 0.16 pm) and the model of the spectrum is a Modified Lorentzian with "n" factor equal to 3.6.

From Figure 11 we can conclude that, depending on the pattern, the laser contribution to the total CDU budget can be about 10%. LINE B is less affected by the laser contribution than the other patterns.

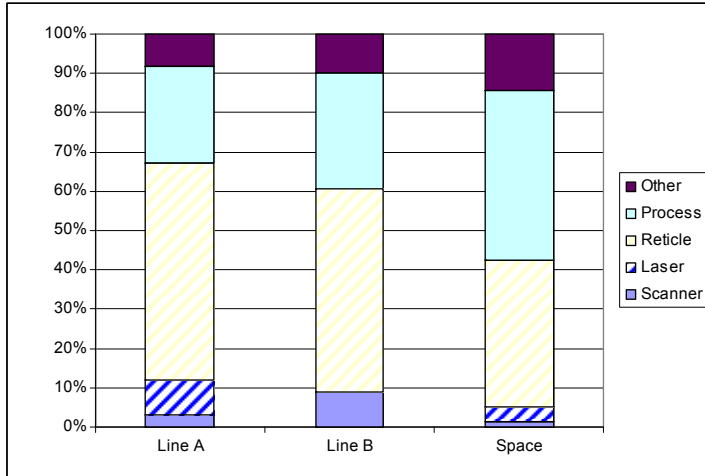


Figure 11: CDU budget for the different patterns and contributors

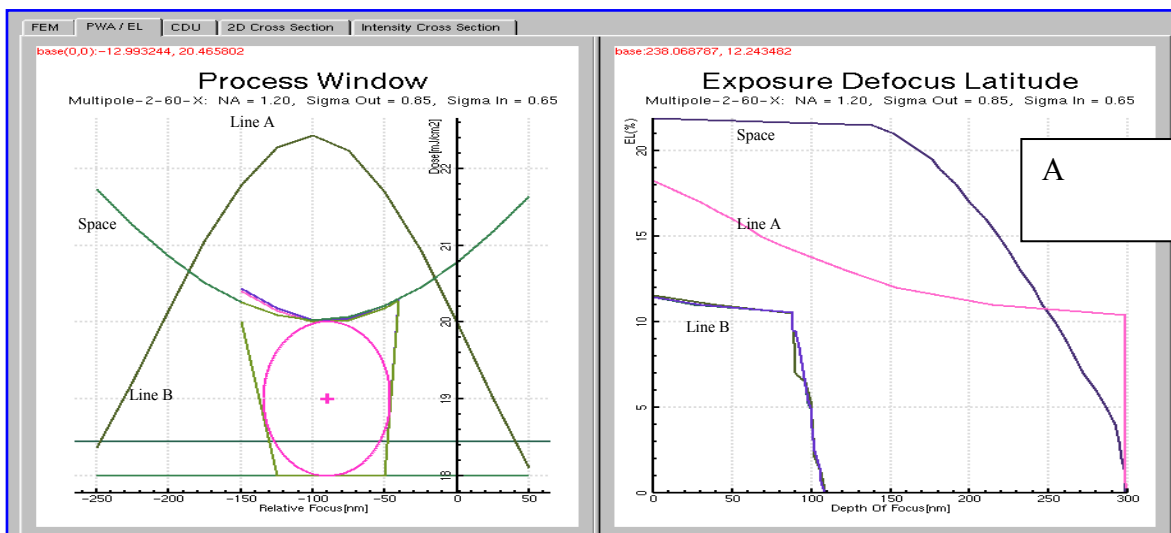
### 2.4 DOF simulation vs Laser Bandwidth

We determined the process window for the 3 different patterns for different typical conditions of the laser bandwidth. The depth of focus and exposure latitude of the overlapping process window is shown in **Table 2**.

Setting	FWHM (pm)	E95 (pm)	DOF (nm)	EL at 10% CD (nm)
A	0.12	0.25	86	19
B	0.22	0.37	64	18
C	0.33	0.5	34	6

Table 2: Elliptical DOF and EL for different laser bandwidth setting of FWHM and E95

Conditions “A” and “B” can be considered as the range of bandwidth used for normal operation. Within this range a consistent DOF reduction of about 14% can be explained by the high sensitivity of the LINE B pattern to defocus as can be seen in Figure 12. We will perform an experiment to confirm these results.



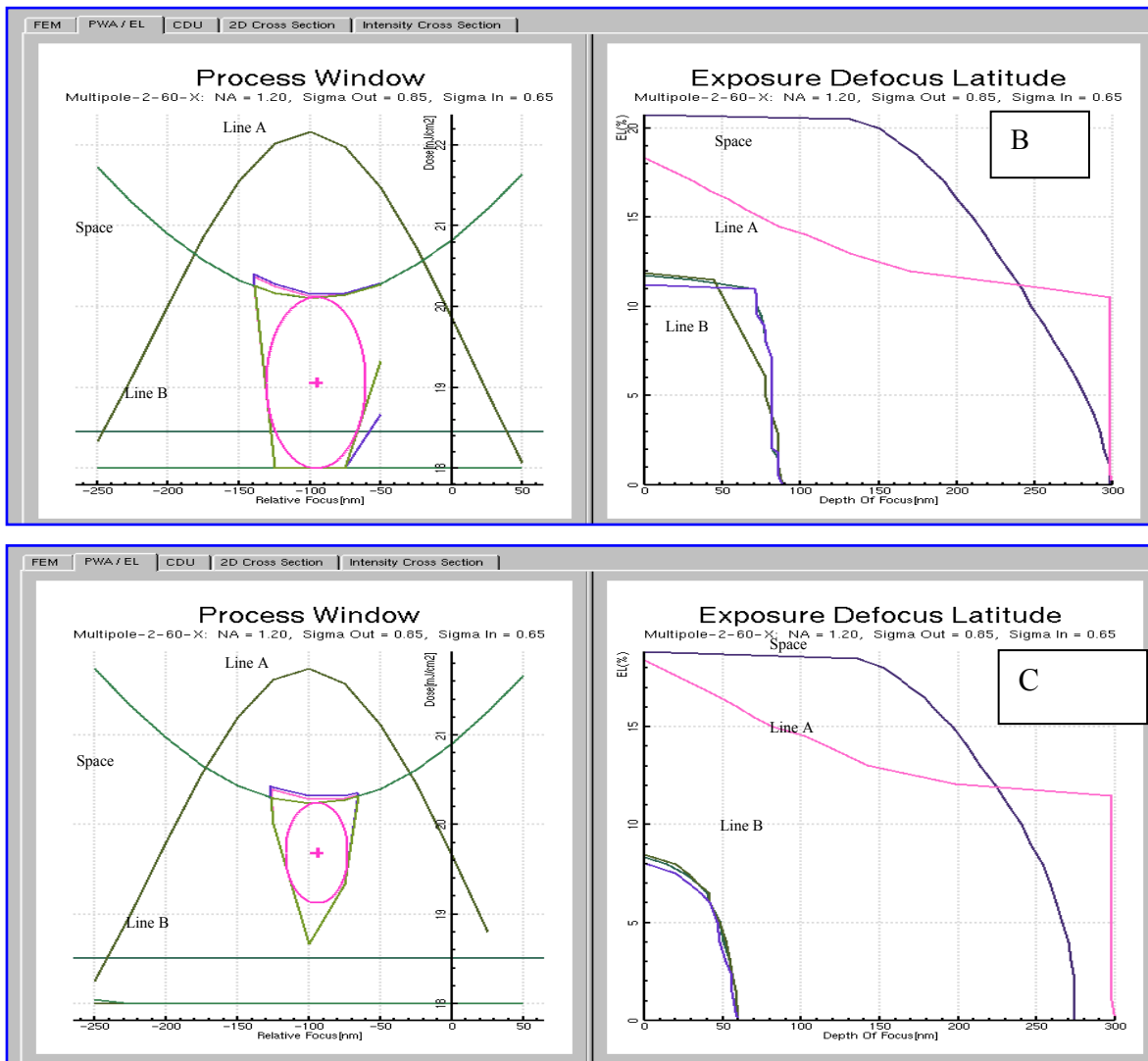


Figure 12: process window plots at different bandwidth settings

### 3. EXPERIMENTAL RESULTS

#### 3.1 Overlay experiment

In order to confirm the simulations, we ran a 2-pass overlay test, where the first (reference) layer is exposed with the nominal wavelength and the second one with a wavelength set-point offset at two WL offset settings (+0.5pm, -0.5pm) in addition to the baseline exposure. According to the simulations, we expect a maximum effect of about 2.5nm through the slit (see Figure 8) for the most sensitive feature, LINE B. The bandwidth of the laser for this experiment is set to  $e95=0.25$ .

Ideally the overlay targets should be representative of standard process monitoring conditions for this technology.

In particular, different types of overlay mark segmentation may exhibit a different sensitivity to chromatic aberrations compared to non-segmented marks. At the same time, the defocus due to longitudinal chromatic aberration may begin to result in contrast loss of segmented marks particularly for higher WL offsets.

The purpose of this test is to extrapolate the shift behavior of different targets with the wavelength in order to convolute the results simulating a bandwidth impact. We will compare the experimental results with the simulations.

### 3.2 Overlay target and sampling description

The experiment described in the previous section was carried out using Advanced Imaging Metrology (AIM) targets with different features size as reported in Figure 13 a) and measured on Archer™ 100IS metrology tool. Dedicated overlay targets sampling plan was introduced in order to catch distortion map across the field and exposure slit as depicted in Figure 13 b) and c) respectively. Full wafer coverage has been considered.



Figure 13: starting from the top: the first 3 rows are AIM targets used for distortion calculation, 2-pass overlay test. The last row shows targets {G, A, E} which are suitable targets to evaluate the imaging fingerprint across the slit. b) Field sampling for 2-pass overlay test. c) Slit sampling for IPE calculation

Except for the {G, A, E} targets, the metrology targets shown in Figure 13 are 2 layers targets where inner and outer gratings of AIM are printed at two different exposure runs. On the contrary, {G, A, E} are single layer AIM targets and printed at the same time in a single exposure run.

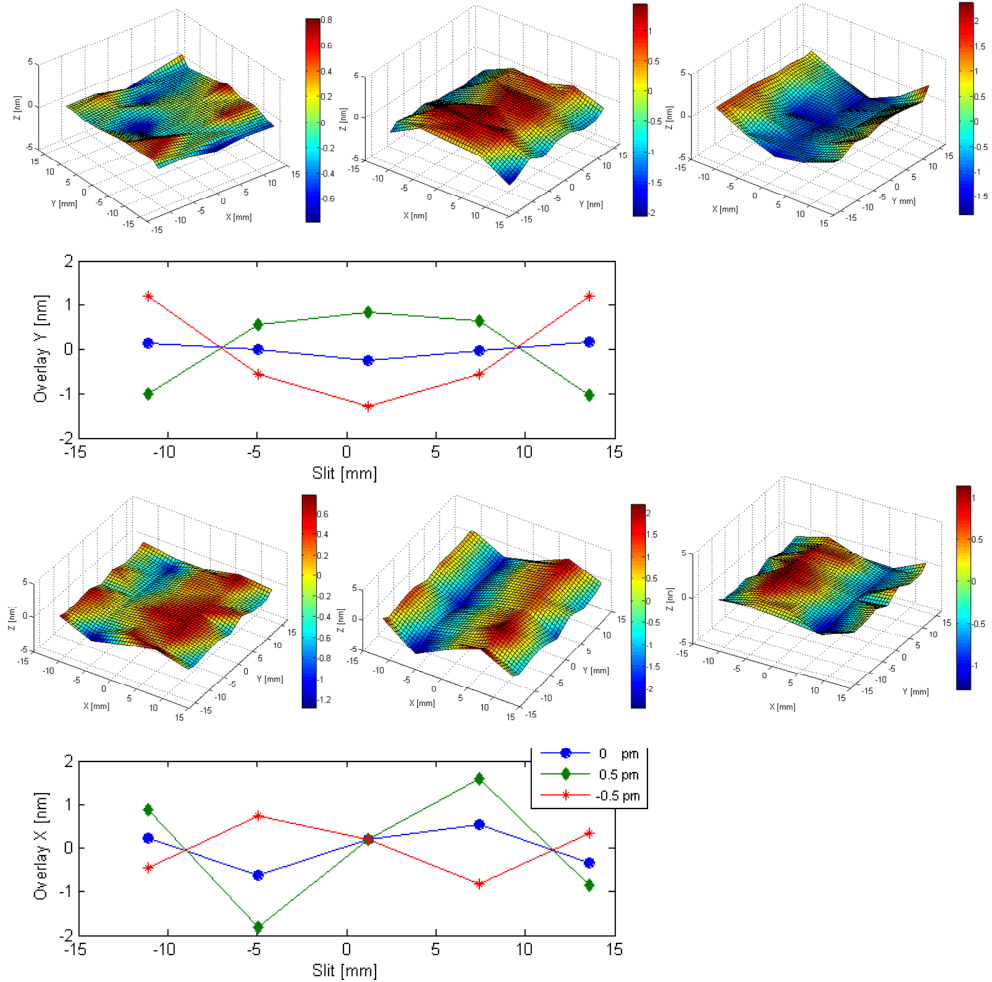
In order to have a reliable characterization of metrology measurements we have estimated the maximum error contribution in terms of Total Measurement Uncertainty (TMU) and random error propagation. The result is  $3\sigma \leq 0.4\text{nm}$ . This is the maximum error bar for both X and Y measurements.

### 3.3 Discussion of the results

The results of metrology measurements, conducted using three different AIM targets as described in the previous section, are presented. As shown later, all measurements using different AIM targets are well matched one to another. Therefore, in Figure 14 only the Non Correctible Errors (NCE) of 13x13 μm AIM targets have been depicted. This match means that the 2-run overlay test is independent from target used for overlay characterization, in particular from feature size of the bar assembling the grating. From Figure 14, it's clearly visible that both NCE in X and Y are a function of the wavelength shift  $\Delta\lambda$ . The effects might be ascribed to non-linear overlay contributions. In particular, the NCE Y appears as a 2<sup>nd</sup> order distortion across the slit whereas the NCE X appears as a 3<sup>rd</sup> order distortion across the slit,

see Figure 14 b), d) respectively. As is obvious, the reference state  $\Delta\lambda=0$  does not have large high order components (however, a small residual 3<sup>rd</sup> order NCE results from the specific illumination mode used). For what concerns the range of variation in terms of peak to valley (p2v) as a function of wavelength shift with respect to the reference state ( $\Delta\lambda=0$ ), we found p2v of NCE X and NCE Y of around 2nm. From the simulation results we also found errors of around 2nm.

Figure 14: a) NCE in the Y direction across the field and through wavelength shift. b) Orthogonal projection of NCE Y onto the exposure slit. c) NCE X direction across the field and through wavelength shift. d) Orthogonal projection of NCE X onto the exposure slit. The NCE is calculated by subtracting the linear model terms from measured data



### 3.4 IPE discussion

Considering two different set of variables, wavelength  $\equiv \{\Delta\lambda=0, \Delta\lambda=0.5, \Delta\lambda=-0.5\}$  and IPE targets  $\equiv \{G, A, E\}$  we are able to evaluate the relative maximum contribution to Image Placement Error. Taking a look at Figure 15 and selecting the most sensitive target the relative maximum contribution to IPE as a function of wavelength is  $\leq 0.1\text{nm}$ . These experimental results are in good agreement with the simulations shown in Figure 4 for the different product patterns (LINE A, LINE B and SPACE). Keeping the wavelength constant, the relative maximum contribution to IPE as a function metrology targets is  $\leq 0.7\text{nm}$ .

As a comparison, a 0.5pm wavelength variation used in these experiments and simulations is over an order of magnitude greater than the laser wavelength stability specification for the XLA 360 generation lasers, and up to two orders of magnitude greater than actual performance for the latest generation XLR lasers.

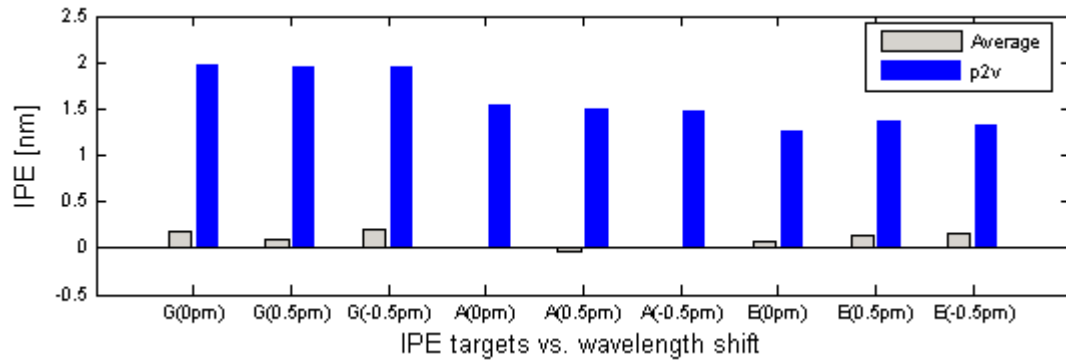


Figure 15: Image Placement Error as a function of metrology targets {G, A, E} and wavelength shift { $\Delta\lambda=0$ ,  $\Delta\lambda=0.5$ ,  $\Delta\lambda=-0.5$ }

### 3.5 IPE simulation with measured Zernikes

To understand the wavelength setpoint effect on overlay we simulate the AIM target shift with the full sets of lens Zernikes collected after each wavelength offset.

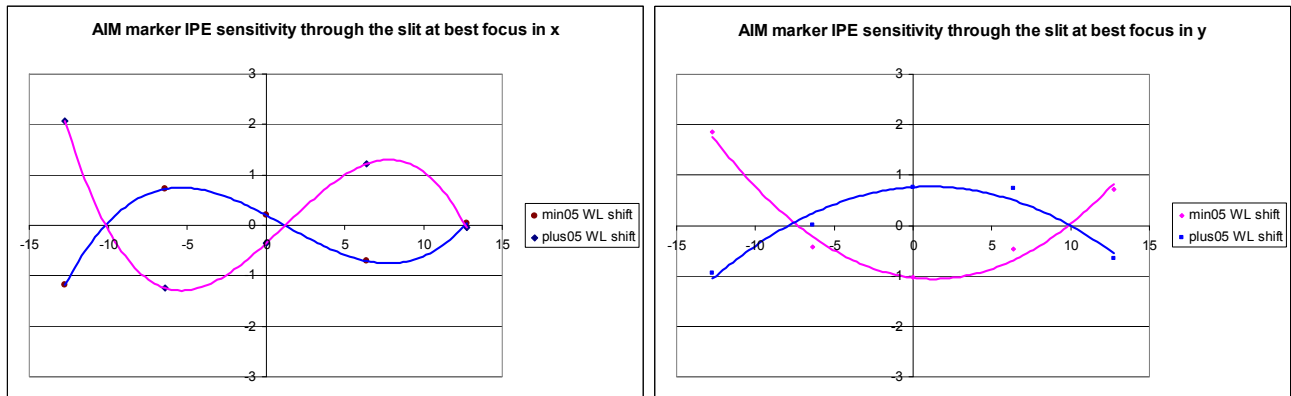


Figure 16: AIM marker IPE sensitivity through the slit

Figure 16 confirms the second order shift in Y and the third order shift in X coming mainly by Z2 and Z3 wavelength sensitivity in the slit.

This effect is not automatically compensated during the exposure inducing a third order in X and second order in Y lens distortion.

These misalignments are anyway perfectly symmetrical with respect to the reference wavelength hence we can conclude that a bandwidth drift considered as a convolution of three wavelengths here analyzed may not significantly impact the lens distortion.

## 4. SUMMARY AND CONCLUSIONS

The work in this paper has shown the IPE resulting from the higher order Zernike terms are small but depend on the feature type. We simulated the effect and followed up with an experiment to confirm the result.

The maximum across slit IPE that we simulated and subsequently confirmed by an experiment is about 2.5nm, 0.7nm and 0.4nm for the LINE A, LINE B and SPACE features respectively. A simulation found that the effect of a bandwidth variation of 0.5pm is about 0.2 nm to 0.5nm for the most sensitive pattern, LINE B, at the defocus extremes. Note that 0.5pm bandwidth variation modelled in this work is significantly higher than controlled in current-generation lasers.

We found that the DOF of the most sensitive pattern, LINE B, is reduced by about 14% within the standard operating range of the laser. This will be confirmed by an experiment. Current-generation lasers are able to control the bandwidth such that the risk of this type of effect is reduced. The CD Uniformity contribution from the laser to the total CD uniformity budget is estimated by dedicated simulations to be less than 10%.

CDU uniformity as a function of bandwidth depends on the type of pattern and the laser contribution is highest for the LINE A feature. These two results show that asymmetric patterns can be sensitive to bandwidth. We note that the XLR 560i and XLR 660ix both offer lower nominal bandwidth operation and significantly lower bandwidth variability due to bandwidth stabilization technology and a new wavelength controller.

Additionally we showed that the IPE is insensitive to the type of overlay measurement mark. We investigated 3 types of marks and found that the maximum difference is less than 0.1nm. This was also confirmed by a simulation.

An investigation of the 32nm pattern found that it is less sensitive to IPE than the pattern shown in Figure 1.

## 5. REFERENCES

- [1] P. Rigolli et al., "AIM technology for Non-Volatile Memories microelectronics devices", SPIE2006, 6152-175
- [2] E. Hendrickx, A. Colina, A. van der Hoff, J. Finders, G. Vandenberghe, Image placement error: closing the gap between overlay and imaging, *J. Microlith., Microfab., Microsyst.* 4(3), 033006 (Jul-Sep 2005)
- [3] P. de Bisschop, I. Lalovic, F. Trintchouk, Impact of finite laser bandwidth on the critical dimension of L/S structures, *J. Micro/Nanolith. MEMS MOEMS* 7(3), 033001 (Jul-Sep 2008)
- [4] M. Smith, J. Bendik, I. Lalovic, N. Farrar, W. Howard, C. Sallee, "Modeling and Performance Metrics for Longitudinal Chromatic Aberrations, Focus-drilling, and Z-noise; Exploring excimer laser pulse-spectra," *Proc. SPIE Optical Microlithography XX* 6520 -127 (2007).
- [5] M.Terry, I. Lalovic, G. Wells, A. Smith, Behavior Of Lens Aberrations As A Function Of Wavelength On KrF and ArF Lithography Scanners, *Proceedings of SPIE Vol. 4346* (2001)
- [6] V.N. Mahajan, *Optical Imaging and Aberrations-II: Wave Diffraction Optics*, SPIE Press, Bellingham (2001)
- [7] I. Lalovic, O. Kritsun, S. McGowan, J. Bendik, M. Smith, N. Farrar, "Defining a physically-accurate laser bandwidth input for optical proximity correction (OPC) and modeling", *Proc. BACUS XXII Photomask Technology Symposium* 7122 -62, (2008).